Two zone transient storage modeling using temperature and solute data with multiobjective calibration: Part 2 Temperature and Solute

B. T. Neilson[a], D. K. Stevens[b], S.C. Chapra[c], C. Bandaragoda[d]

[a]Utah State University, Civil and Environmental Engineering, Utah Water Research Laboratory, 8200 Old Main Hill, Logan, UT 84321, USA, bethany.neilson@usu.edu, 435-797-7369

[b] Utah State University, Civil and Environmental Engineering, Utah Water Research Laboratory, 8200 Old Main Hill, Logan, UT 84321, USA, david.stevens@usu.edu, 435-797-3229

[c]Tufts University, Civil and Environmental Engineering, 113 Anderson Hall, Medford, MA 02155, USA, steven.chapra@tufts.edu, 617-627-3654

[d] Silver Tip Solutions, 10623 56th Ave W, Mukilteo, WA, 98275, USA, christina@silvertipsol.com, 425-501-4191

Two zone transient storage modeling using temperature and solute data with multiobjective calibration: Part 2 Temperature and Solute

B. T. Neilson, D. K. Stevens, S.C. Chapra, C. Bandaragoda

Abstract

This paper presents the multi-objective calibration results for temperature and solute of a two-zone temperature and solute (TZTS) model which separates transient storage into surface (STS) and subsurface (HTS) transient storage components. This model contains terms associated with surface heat fluxes in the MC and STS, heat and mass exchange between the STS and MC, heat and mass exchange between the HTS and MC, and heat exchange due to bed and deeper ground conduction. To estimate the additional parameters associated with a multiple-zone model, a data collection effort was conducted to provide temperature time series and solute tracer curves representing the movement of heat and/or solute through each zone. A multi-objective calibration algorithm was linked to the TZTS model to assist in parameter estimation and provide information about parameter uncertainty and tradeoffs associated with matching different combinations of observations (e.g., solute and/or temperature data gathered in various zones). Results generated from three different combinations of calibration data illustrated that the two-zone model accurately reproduces temperatures and tracer concentrations observed in different zones when considered independently. However, there were many parameter sets that resulted in objectively indistinguishable results. When tracer and temperature observations were

considered simultaneously in model calibration, the simplistic representation of the surface and subsurface zones do not adequately reproduce both observation types in each zone. If the uncertainty in model parameters and the data are taken into account, however, the results of the study suggest that it is plausible to use temperature and tracer information simultaneously to better inform transient storage modeling approaches.

Key words: hyporheic, two-zone modeling, instream temperature modeling, tracer, multi-objective optimization

Index terms: (1814) Energy budgets, (0414) Biogeochemical cycles, processes, and modeling, (1878) Water/energy interactions, 1873(Uncertainty assessment)

Introduction

The importance of hyporheic and other types of storage in streams have been of interest due to their effects on the fate and transport of constituents through hydrologic systems [*Chapra and Runkel*, 1999; *Jones and Mulholland*, 2000]. It is understood that constituent behavior in the hyporheic and surface storage zones will differ because subsurface zones can become anoxic while the surface zones are more likely oxic [*Runkel and McKnight*, 2003]. Additionally, sorption (e.g., metals [*Zaramella et al.*, 2006]) and/or uptake (e.g., organic carbon processing by microorganisms [*Battin et al.*, 2008]) of some constituents within the subsurface decreases transport rates. Temperature within each of these zones, which affects reaction rates and influences main channel temperatures, will also differ because the surface storage is exposed to the atmosphere [*Neilson et al.*, 2009; *Runkel and McKnight*, 2003].

The combination of the hyporheic storage, dead zones, and other slow-moving water relative to the main channel flow have been collectively termed "transient storage" [*Bencala and Walters*, 1983]. The mechanisms of transient storage have typically been approximated in the context of an advection-dispersion model of one-dimensional solute transport including first-order exchange into the storage zone [*Bencala and Walters*, 1983; *Runkel*, 1998]. This type of model requires estimation of parameters corresponding to the extent or volume of the storage and exchange rates that are typically estimated from solute tracer experiments. This stream-tracer approach to modeling solute transport lumps the surface transient storage (STS) and hyporheic transient storage (HTS) into one zone (i.e., a one-zone stream solute model) and, therefore, does not distinguish between surface or subsurface storage processes [*Harvey and Wagner*, 2000;

Runkel and McKnight, 2003]. Although the one-zone transient storage modeling has proven to provide realistic characterization of several storage processes lumped into one [*Choi et al.*, 2000], multiple zone models have been developed and are more commonly being used to quantify the individual effects of storage zones with different characteristics [*Briggs et al.*, 2009; *Choi et al.*, 2000; *Harvey et al.*, 2005]. While these models may be able to separate the surface and subsurface storage, they still provide an average, simplistic representation of the broad spectrum of storage sizes and rates of exchange. The common assumption of first order exchange within storage zone models results in an exponential distribution of residence times within each zone [*Harvey et al.*, 1996]. Many have shown this assumption to be inappropriate for some study areas and have found other types of distributions that better characterize observed residence time distributions [*Cardenas et al.*, 2008; *Haggerty et al.*, 2002; *Worman et al.*, 2002].

The typical stream tracer approach to estimating the influence of transient storage on solute transport includes collection of tracer data in the main channel at a number of longitudinal locations [*Bencala and Walters*, 1983; *D'Angelo et al.*, 1993; *Laenen and Bencala*, 2001; *Worman et al.*, 1998] but has included sampling in the hyporheic zone [*Harvey et al.*, 2005; *Worman et al.*, 1998], and throughout transects in a wetland [*Harvey et al.*, 2005]. Recently, however, Briggs et al. [2009] proposed that additional tracer data be collected in representative STS zones to assist in parameter estimation associated with two-zone modeling. Beyond collection of data from various storage zones, Zaramella and Packman [2003] and Harvey and Wagner [2000] point out that there are limitations in using only tracer experiments to determine meaningful information about the surface and subsurface processes. While stream-tracer experiments provide information about time scales of storage, it is important to collect complementary information about subsurface processes [*Harvey and Wagner*, 2000].

As discussed in Neilson et al. [2010], when adding another storage zone to any model formulation, the resulting increase in the number of parameters requiring estimation and the associated data collection required to support parameter estimation is challenging. Additionally, the increase in the number of parameters requires the identification of an appropriate and robust calibration approach. Similar challenges have been faced in hydrologic modeling due to large numbers of parameters and limited data. Optimization algorithms, including the Shuffled Complex Evolution (SCE-UA) algorithm [*Duan et al.*, 1992] and Shuffled Complex Evolution Metropolis (SCEM-UA) algorithm [*Vrugt et al.*, 2003a]), have been developed to support hydrologic model calibration and base their search on minimizing a single objective function (e.g., root-mean-square error (*RMSE*), mean absolute error (*MSE*), bias, Nash-Sutcliffe Efficiency (*NSE*), etc.) or 'goodness-of-fit' measure [*Legates and McCabe*, 1999]. The Multi-objective Shuffled Complex Evolution Metropolis (MOSCEM) algorithm [*Vrugt et al.*, 2003b] was built on the SCEM-UA global optimization algorithm, but uses the concept of Pareto dominance to address multiple objectives due to the limitations associated with using only one objective function. When using single or multiple objective optimization algorithms, the data used in the calculation of the goodness-of-fit measure may need to represent different characteristics of the system to result in the best estimates of the parameters.

In this paper we present a two zone temperature and solute (TZTS) model case study from the Virgin River, UT. We investigate the utility of using different data types and various sampling locations by building on Neilson et al. [2010]. We expand on past solute injection methods of estimating the effects of transient storage through use of both heat and solute information to inform transient storage parameter estimates. Additionally, we provide an initial understanding of parameter uncertainty in the two-zone modeling application through use of

MOSCEM. The utility of this multi-objective calibration algorithm coupled with the TZTS model is discussed based on the results of three different two objective calibrations that use various data types (e.g., tracer solute and/or temperature data gathered in various zones). Data not employed in the calibration that represent different locations or storage zones were used to test and corroborate model.

Two-Zone Temperature and Solute Model Formulation: Solute Equations

The TZTS temperature model formulation is described in detail in Neilson et al. [2010]. The solute portion of the model (Eqns. 1-3) is similar to the temperature portion, but the mass balance equations are simpler due to fewer sources and sinks relative to heat.

$$\frac{\partial C_{MC}}{\partial t} = -U_{MC}\frac{\partial C_{MC}}{\partial x} + D\frac{\partial^2 C_{MC}}{\partial x^2} + \frac{\alpha_{STS} Y_{STS}}{A_{cs,MC} B_{STS}}(C_{STS} - C_{MC}) + \frac{Q_{HTS}}{V_{MC}}(C_{HTS} - C_{MC}) \quad (1)$$

$$\frac{dC_{STS}}{dt} = \frac{\alpha_{STS}}{(\beta B_{tot})^2}(C_{MC} - C_{STS}) \quad (2)$$

$$\frac{dC_{HTS}}{dt} = \frac{Q_{HTS}(C_{MC} - C_{HTS})}{Y_{HTS} A_{S,MC}} \quad (3)$$

where C = concentration (mg/L), Q = volumetric flow rate (m^3/s), V = zone volume (m^3), D = longitudinal dispersion (m^2/d), Δx = volume length (m), α_{STS} = exchange between the main channel and the surface transient storage (m^2/d), Q_{HTS} = hyporheic transient storage advective transport coefficient (m^3/d), A_{cs} = cross-sectional area of zone (m^2), B_{tot} = total volume width (m), β = the surface transient storage fraction of the total channel width, Y_{HTS} = depth of hyporheic zone (m), t is elapsed time (days), and $A_{S,MC}$ = surface area of interface between hyporheic zone and main channel (m^2). The subscripts *MC*, *STS*, and *HTS* specify the main channel, surface transient storage, and the hyporheic transient storage, respectively.

As detailed in Neilson et al. [2010], model assumptions include completely-mixed reaches and storage zones; steady, non-uniform hydraulics; MC advection and dispersion; one-dimensional first-order mass transfer from the HTS and STS zones across an interfacial area with the MC; hyporheic zone width set to the MC width; analogous mass and heat exchange rates; and bed conduction between the MC water column and bed sediments and the STS water column and bed sediments.

When Δx is specified, there are five free parameters associated with the two transient storage zones ($Q_{HTS,i}$, $Y_{HTS,}$, $\alpha_{STS,i}$, $A_{cs,STS}$, β). Since heat and mass transfer are treated analogously, these parameters are the same for solute and temperature calculations. Additional parameters necessary to calculate the heat fluxes include the depth of the ground conduction zone (Y_{gr}) and those associated with bed and ground conduction (sediment density (ρ_{sed}), heat capacity ($C_{p,sed}$), and coefficient of thermal diffusivity (α_{sed})). Beyond these parameters, the channel widths (B_{tot}), longitudinal dispersion (D), and Manning's roughness coefficient (n) may also vary in the modeling reaches. As discussed in Neilson et al. [2010], B_{tot} and n are allowed to vary within reasonable bounds measured in the field, but D was estimated and held constant.

Methods

Site Description and Data Collection

Neilson et al. [2009 and 2010] provide details regarding the 18 km long study reach and data collection points. Cross Section 1 (CS 1) is the upper boundary of the study reach, CS 2 is located 11 km below CS 1 and CS 3 (the terminus of the study reach) is 18 km below CS 1. Due to bottom slope and substrate differences, the study reach has been split into two sections that have the potential to function differently in terms of surface and subsurface transient storage. Section 1, includes the reaches between CS 1 and a part of the river 1.75 km below CS 2, and Section 2 includes CS 3. In order to support parameter estimation associated with this two-zone model, solute tracer and temperature data were collected from the main channel and within the storage zones where possible. Information regarding the temperature data and the locations where these data were collected are provided in Neilson et al. [2009 and 2010].

The addition of solute data in model calibration allows for a second type of tracer past temperature and provides more calibration data (both temporally and spatially). In this study, a sampling approach similar to Briggs et al. [2009] was implemented for solute tracer data collection where data were collected both in the MC and in two representative STS zones (representing the surface storage) near CS 3. These representative locations were chosen based on previous tracer study observations where an injected dye tracer would be trapped and slowly bleed back into the MC. As with the Briggs et al. [2009] study, it was anticipated that based on understanding of the STS and MC tracer response, the behavior of the HTS zone could be

extracted. For this tracer study, a 300 g instantaneous pulse of fluorescent Rhodamine WT dye was injected at 12:30 pm at the head of a riffle just upstream of CS 1. A Self-Contained Underwater Fluorescence Apparatus (SCUFA) (Turner Designs, Sunnyvale, CA) was deployed in the main flow of the channel at CS 3 and measurements were taken every ten seconds for approximately six hours. Grab samples were also collected near the SCUFA to provide an independent measure in the MC and in the two representative STS locations. The grab samples were immediately analyzed in the field using a Turner Model 450 lab fluorometer (Turner Designs, Sunnyvale, CA).

Especially when using non-conservative tracers like Rhodamine WT, there are many sources of uncertainty associated with the tracer results. These include the influences of turbidity on measurements, inappropriate instrument calibration and general instrument error; and loss of Rhodamine WT due to photodegradation, sorption to streambed sediments (mineral and organic), reaction in solution, volatilization, and uptake by living organisms [*Bencala et al.*, 1983]. In this study, significant loss of Rhodamine WT due to sorption was less of a concern because the organic matter content in the bed sediments was extremely low (averaging 0.05% at four sampling locations). A recent sorption study [*Bingham*, 2009] at four sampling locations along this stretch of the Virgin River resulted in an average K_d value of 1.5 mL/g, which is relatively low based on other Rhodamine WT sorption studies found in the literature [*Bencala et al.*, 1983; *Everts and Kanwar*, 1994; *Lin et al.*, 2003; *Shiau et al.*, 1993].

To ensure that the reach length associated with the tracer study was appropriate, we calculated the Dahmköhler number (*DaI*) [*Wagner and Harvey*, 1997] for a one zone version of the model calibrated to the MC tracer response at CS 3. The DaI is defined as:

$$DaI = \frac{\alpha_{OTIS}(1 + A_{c,MC} / A_{c,TS})L}{v} \quad (4)$$

where α_{OTIS} = transient storage exchange coefficient (s-1) [*Bencala and Walters*, 1983; *Runkel*, 1998], $A_{c,MC}$ = cross sectional area of the MC, $A_{c,TS}$ = cross sectional area of the transient storage zone, L = length of stream reach over which tracer study is conducted, and v = average velocity of stream reach. Using the relationships between α_{OTIS} and α_{STS} for the TZTS model [*Neilson et al.*, 2010], an appropriate *DaI* equation can be established for the TZTS model parameters.

TZTS Parameter Bounds

As discussed in Neilson et al. [2010], model simulations were conducted using Latin Hypercube parameter sampling to define the feasible parameter space for optimization and to establish relationships between the various data types and sampling locations. The 15 parameters consisted of the seven calibration parameters identified previously (β, $A_{c,STS}$, α_{STS}, Y_{HTS}, Q_{HTS}, B_{tot}, n) for Section 1 and Section 2, and Y_{gr} which is assumed to be the same for both Section 1 and Section 2. The *NSE* was the objective function calculated from observed and predicted time series of temperature and solute and was the basis for setting the appropriate parameter bounds for optimization. The subset of observations selected arbitrarily for use in the sensitivity analysis included the MC temperatures at CS 2, MC temperatures at CS 3, and MC and STS solute concentrations at CS 3. *NSE* values were calculated for each of these time series for 6000 simulations. *NSE* values greater than 0.9 for each individual observed time series and the corresponding parameter sets were defined as acceptable. All acceptable parameter sets were

pooled to establish the parameter bounds for optimization. An *NSE* value of 0 implies that the model gives no more information than a simple mean. The results from this exercise served not only provide parameter bounds for the optimization algorithm, but also provided information regarding the relationships between temperature and solute predictions.

TZTS Model Calibration Using MOSCEM

As discussed in Part 1 of this paper [*Neilson et al.*, 2010], MOSCEM uses the concept of Pareto dominance to determine the optimal parameter sets based on multiple objectives. Vrugt et al. [2003b] state that incompleteness or errors in model structure and errors in the data can prevent the occurrence of a parameter set where all objective functions have their minima. Therefore, a Pareto solution represents a parameter set that is impossible to distinguish as being objectively better than any other Pareto solution in the absence of more information [*Gupta et al.*, 1998].

With the parameter bounds established by the sensitivity analysis, the TZTS model was calibrated by minimizing (1-*NSE*) for two data sets simultaneously using MOSCEM for three different cases. The first case minimized the objective function (1-*NSE*) for MC temperatures at both CS 2 and CS 3 (as shown and discussed in Neilson et. al. [2010]). The second case used the objective function (1-*NSE*) for the MC and STS tracer concentrations. The third case used the objective function (1-*NSE*) for the MC tracer concentrations and MC temperatures at CS 3. For each of the three two-objective optimization runs, Pareto fronts were plotted and the optimal tradeoffs were found by determining the Pareto solution with the smallest Euclidean distance

from the origin. The corresponding parameter set was selected as the compromise that represents both objective functions.

Results

Tracer Study Results

Figure 1 shows the tracer data collected at CS 3 in the Virgin River MC and two STS locations. STS 1 was in a much slower moving portion of the flow in the river. STS 2 was located in a small stagnant zone near the edge of the stream. The results from STS 1 show that the rising portion and the beginning of the falling portion of the curve are similar to that in the MC. The curves diverge in the bottom portion of the falling portion as it transitions to the tail. This divergence at the tail suggests that in this type of STS, the exchange is fast when there is a high concentration gradient and slower when there is a low concentration gradient. The results from STS 2 show a lag earlier in the falling limb and a larger difference in the tail initially. This is likely due to STS 2 being located further from the MC flow. In general, the STS and MC behavior in this system appear to be similar, so the transient storage represented by the tracer tail is likely dominated by subsurface storage.

The average flow rates in Section 1 and Section 2 are 2.86 and 3.15 $m^3 s^{-1}$, respectively. The tracer study was conducted over the entire 16.5 km study reach. With the parameters associated with a one zone calibration (Table 1), *DaI* values were calculated for each section. These calculations provide a range of the possible *DaI* values by assuming that the parameter set

associated with each section would hold for the entire 16.5 km portion of the study reach. The values of 1.8 and 1.1 suggest that the study reach was an appropriate length.

TZTS Parameter Bounds

Objective function values calculated from observed and predicted time series of tracer concentrations and temperatures were the basis for setting the appropriate parameter bounds (shown in Table 2 in *Neilson et al.* [2010]) for use in optimization. Another benefit of the sensitivity analysis was the ability to use the parameter sets corresponding with $NSE > 0.9$ for each data set (e.g., MC temperature at CS 2, MC temperature at CS 3, and so on) to analyze the corresponding model results for the other locations and constituents. For example, for all parameter sets associated $NSE > 0.9$ for MC temperature at CS 2, model results can be plotted for CS 3 temperature and solute versus actual observations in these zones. This allowed an initial understanding of the relationships between locations (CS 2, CS 3, MC, STS) and/or tracer types (conservative solute versus temperature).

First, the parameters sets corresponding to $NSE>0.9$ were calculated from the model results and observations for MC temperatures at CS 2. The model simulations using these parameters sets resulted in bounds (shaded areas) associated with each data type and location (Figure 2). Figure 2a shows the narrow bounds associated with the $NSE > 0.9$ for MC temperatures at CS 2. Figure 2b shows the MC temperatures estimated for CS 3 and suggests that a good fit at CS 2 will support a good fit at CS 3. Tracer estimates at both CS 2 and CS 3 (2c and 2d), however, are highly variable and suggest that the MC temperature data at CS 2 do not provide adequate information regarding the tracer behavior at CS 3 in the MC or STS.

Similarly, model simulations using accepted parameter sets for observed MC temperatures at CS 3 are presented in Figure 3. Figure 3b shows that the predictions for the MC at CS 3 do not include the data in portions of the diel cycle; however, the bounds on the predictions are narrow. Figure 3a shows that MC temperatures at CS 2, are accurately predicted using these parameters based on observations at CS 3. Tracer estimates at CS 3 (3c and 3d), are again, however, quite variable. Therefore, the MC temperature data at CS 3 does not provide enough information about the behavior of the tracer at CS 3.

Figure 4 shows the model simulations resulting from $NSE > 0.9$ for tracer data from the MC at CS 3. Figures 4c and 4d show that the model bounds are now narrower around both sets of tracer observations and suggest that the behavior in the MC and the STS at CS 3 are dependent. Figures 2 and 3 showed that solute tracer behavior was not easily inferred from temperature information. Figures 4a and 4b, however, indicate that by fitting the model to tracer results at CS 3, MC temperatures at CS 2 and 3 are reasonably represented. Nonetheless, the minimum temperatures are consistently underestimated and the bounds of the temperatures are much greater than those which are obtained by using temperature data directly. Simulations associated with the STS tracer at CS 3 resulted in similar bounds as those shown in Figure 4.

TZTS Model Calibration Using MOSCEM

Figures 5, 7, and 8 show the model results based on the optimal parameter set from the calibration. Each subplot (a-h) shows the model results and observations for each constituent, zone, and location being modeled. Observations and model results are shown for the zones not being used in the optimization to corroborate whether the resulting parameter sets from each

calibration provides an accurate representation of the exchange and storage processes for each zone at the reach scale.

Figure 5 shows the model output for the best parameter set resulting from the optimization of (1-*NSE*) for the MC temperatures at CS 2 and (1-*NSE*) for the MC temperatures at CS 3. Figure 5a and 5b show the results for the MC temperatures at CS 2 and CS 3, respectively, which were the time series used in calibration. As discussed in Neilson et al. [2010], the predicted temperatures for the MC in CS 2 match the observations well; however, the temperatures are underestimated in CS 3 after approximately 0.3 days. Figure 5d and 5e show the results for the STS at CS 2 and 3, respectively. Both the river left (solid black line) and river right (dashed black line) STS observations are additionally plotted for both CS 2 and 3. Figure 5d shows that the STS temperatures nearly match the two sets of observations. CS 3 STS temperatures (Figure 5e) match the peak of the river right observations the first day, and then follow the river left the following day. The minimum temperatures, similar to the MC, are slightly underestimated.

Figure 5g and 5h show that the HTS predictions are within the bounds of the three depths of HTS temperature observations shown in black (solid line = 3 cm deep, dashed line = 9 cm deep, and dotted line = 20 cm deep). The HTS temperatures at CS 3 (Figure 5h), however, lie within the bounds of the three depths of observations for the first 0.5 days until the temperature probes were buried by moving sand. At 1.3 days, these probes were uncovered, and had to be relocated where the sand was less likely to shift.

The tracer concentrations at CS 3 from this calibration parameter set are significantly underestimated at the peaks and result in a very long tail (only partially shown in this plot). Additionally, the tail of the MC tracer curve was slightly overestimated. In the STS, however,

the tail was fairly similar to that observed. This led to the conclusion that, similar to what was shown in the sensitivity analysis, the MC temperatures alone do not provide enough information to completely understand solute exchange and transport within each zone.

Although the "best" compromise solution was chosen, it is important to highlight that all the parameter sets along the Pareto front are indistinguishable from each other in terms of their ability minimize both objective functions. Figure 6 shows the bounds corresponding to all the parameters sets associated with the Pareto front for the first case, MC temperatures at CS 2 and CS 3. All the temperature plots (a, b, d, e, g, and h) show that there are very narrow temperature bounds associated with the Pareto solutions. The tracer bounds are slightly larger, but still do not provide a solution that matches the tracer observations.

Figure 7 shows the results using parameter sets from the second case that used objective functions associated with MC and STS tracer concentrations at CS 3. It is clear from this figure that tracer concentrations in the STS and MC at CS 3 did not provide enough information concerning the parameters required for estimating temperatures well. This is due in part to the temperature specific parameter Y_{gr}, the depth of the ground conduction layer, that controls the temperatures in the HTS and to some extent, the MC. The tracer data provide no information relevant to estimating this parameter and therefore, it is not estimated well and results in simulated temperature fluctuations that do not match the observations.

The bounds for the Pareto solutions for tracer concentrations in the MC and STS in CS 3 are very narrow and similar to the results shown in Figure 7. Therefore, using the parameter sets associated with good tracer simulations result in poor temperature estimates because the observations do not provide enough information to estimate all 15 parameters

well. This led to the selection of the two objectives in the final calibration of MC tracer concentrations and temperatures at CS 3.

Figure 8 shows the optimal Pareto set results for this case. The results show that a compromise between the MC tracer and temperature results in temperature predictions that are only marginally less accurate than in the temperature-only calibration and tracer concentration predictions that are only slightly lower in the peak and tail compared to the tracer only calibration. Figures 8g and 8h show that a compromise between the MC tracer and temperature results in HTS temperatures that more closely match the observed temperatures 20-cm deep in the sediment versus the average of these sediment probes.

Figure 9 shows the results of all Pareto solutions for the temperature and tracer tradeoff. The ranges associated with the surface temperatures are narrow, but do not provide an accurate estimation of the temperature extremes and do not bracket all the observations. The ranges associated with the subsurface temperatures, however, are broader and successfully bracket many of the observations. The tracer results also have a broad range, but do not capture the peak tracer observations. The tails of the tracer data in both the MC and STS are captured. Table 2 shows the optimal parameter sets for each of the three optimization runs.

Discussion

From the results presented in Figures 5 and 6, it is clear that temperature data in the MC do not provide meaningful information about tracer behavior. This is partially due to many other factors affecting temperatures in each zone that do not influence solute behavior and affect the ability to identify parameter sets. The limited spatial representation of the extent of and

exchange with the complex storage zones may also be a factor. Although the number of temperature time series collected is relatively large, they still do not represent the spatial variability present in the system. For example, both the STS and MC experience surface fluxes that are key in forcing temperature fluctuations in these zones. Recent thermal imagery of this portion of the Virgin River show the surface area associated with the STS are highly variable along the study reach. In contrast to these areas influenced by surface fluxes, the HTS zone experiences a large distribution of hyporheic flow paths and variability in the thermal properties of sediments which affect the heat fluxes occurring in this zone.

Similarly, tracer data alone in the MC and STS do not provide enough information about temperatures in each zone as shown in Figures 7. It is important to point out that the tracer observations did not represent the entire tail of the tracer which limited the information provided about the storage zone behavior. Additionally, one of the most important parameters that affect the overall behavior of temperature in the sediments is the depth of the ground conduction layer (Y_{gr}). The tracer data provide no information about this parameter, so the optimization algorithm cannot determine a consistent estimate of this parameter. As mentioned in Neilson et al. [2010], additional supporting data (e.g., >1 m deep temperature measurements in the bed substrate to provide a lower boundary condition) could decrease the parameter space being sampled by establishing a boundary condition at a specified depth. It is felt that shrinking the parameter space would result in the temperature and tracer results being more analogous and should be investigated further.

The option of using both MC temperature and tracer data at CS 3 provides a compromise by using information about the tracer and temperature behavior. Nevertheless, as shown in Figures 8 and 9, a gain in temperature accuracy results in a loss in terms of tracer accuracy. In

order to ensure that the surface and subsurface zone processes are being represented consistently, the parameters of greatest concern are the exchange coefficients and volume associated with the STS and HTS. As shown by the optimal parameter sets (Table 2) for each of the three optimization runs, when using tracer data only, the STS exchange coefficient (α_{STS}) in the upper section is small relative to the other two optimization runs. When using both temperature and tracer data in the optimization, α_{STS} is high in the lower section relative to the other cases.

The hyporheic storage advective transport coefficient (Q_{HTS}) also varies between scenarios. Using MC temperatures at CS 2 and 3, the transport coefficient in both the upper and lower section is very high and results in a time lag in the MC temperatures [*Neilson et al.*, 2009]. Using only tracer information, the values are significantly lower. Using temperature and tracer information, the values are a compromise and are similar to the tracer values in the upper reach and similar to the temperature values in the lower reach. If solute data were available at CS 2, the appropriateness of this compromise solution could be further tested. Based on this information, concurrent temperature and tracer data should be collected at multiple locations longitudinally in order to inform parameter estimation and corroboration of the model results in each of the zones.

The STS and HTS parameters related to volumes also differ for each optimization run. When only MC temperatures are used, the estimated volume of the HTS is large for each reach in both the upper (218 m^3) and lower (338 m^3) section. The volume of the STS for each reach is 62 m^3 for the upper section and 16 m^3 for the lower section. When using tracer data only, the HTS volume is 30 m^3 for the upper section and 429 m^3 for the lower section. The STS volumes for each reach are 29 and 17 m^3 for the upper and lower section, respectively. When using

temperature and tracer information, the HTS volumes change to 97 and 568 m^3 for the upper and lower section, respectively, and the STS volumes change to 61 and 60 m^3, respectively. Each parameter set results in values of the exchange and volume of storage in the surface and subsurface that are quite different. It is interesting that the total volumes of storage in each reach (i.e., the sum of the HTS and STS in both sections) are 634 m^3 for the temperature optimization, 506 m^3 for the tracer optimization, and 787 m^3 for the temperature and tracer optimization runs. The amount of storage predicted using both the tracer and temperature information is higher than the amount for the other two optimization runs, but they are still similar.

The Pareto front and tradeoff resulting from these simulations imply that the model does not perfectly represent the system. It is likely that a primary reason for this tradeoff is the simplified, one-dimensional, discrete representation of the three dimensional flow continuum in the channel and the associated interactions with the heterogeneous surface and subsurface storage zones that result in varied flow path distributions. As mentioned previously, one simplifying assumption was that of first order exchange between the MC and each of the storage zones. The resulting reach scale model averages the various types and sizes of storage zones that have highly variable timescales of exchange. This assumption, and the resulting exponential residence time distributions, have been shown to provide an inadequate representation of residence time distributions in some systems [*Gooseff et al.*, 2003; *Harvey et al.*, 1996; *Zaramella and Packman*, 2003] and therefore, may also be contributing to the tradeoff.

We believe that the use of multiple data types will provide more information regarding the complexity and spatial resolution necessary within these models to more accurately represent storage zones. The ability to collect high resolution temperature data using distributed temperature sensing (DTS) systems [*Selker et al.*, 2006a; *Selker et al.*, 2006b; *Westhoff et al.*,

2007] or high resolution thermal imagery [*Dunckel et al.*, 2009; *Loheide and Gorelick*, 2006; *Torgersen et al.*, 2001] will greatly support these efforts and make the associated data collection feasible. Additionally, further investigation regarding the data types that provide the most information for parameter estimation will further the use of temperature and solute information to better understand storage zone behavior.

Conclusions

This paper illustrates the utility of multiple data types and in-situ observations from each storage zone in improving parameter estimation associated with two zone modeling. Additionally, this study highlighted the utility of a multi-objective calibration algorithm as a way to identify parameter sets that are indistinguishable in terms of the objective functions of interest and provide information regarding tradeoffs.

Results from using three different combinations of calibration data illustrated that the TZTS model predicted temperatures well in each zone when using MC temperature information at two locations longitudinally in calibration. The associated tracer predictions in MC and STS zone, however, were poor. Similarly, tracer concentrations in the MC and STS were reproduced well when these data were used in multi-objective calibration, however, the associated temperature predictions were inadequate. When tracer and temperature observations were considered simultaneously in model calibration, we found that the simplistic representation of the surface and subsurface zone processes does not perfectly reproduce both types of observations in each zone. If the uncertainty in model parameters and the data are taken into account, the results of the study suggest that it is plausible to combine temperature and tracer

information to better inform two zone modeling approaches. There is, however, an obvious trade-off between modeling solute concentration and temperatures in the Virgin River case study location warranting further investigation of the conceptual model and the associated assumptions, data collection, and the calibration approach. We believe that the use of both solute and temperature information could provide further information regarding the appropriate complexity and spatial scales of modeling and monitoring necessary to further our ability to capture the behavior of these storage zones.

Acknowledgements

We would like to acknowledge the Graduate Assistance for Areas of National Need (GAANN) fellowship that funded this research. We are indebted to our field crews (Quin Bingham, Andrew Neilson, Amber Spackman, Kiran Chinnayakanahalli, Tenielle Beckstead, Jeremy Butterbaugh). We would also like to thank Steve Meismer at the Washington County Water Conservancy District, Rick Fridell and Amos Rehm at the Utah Division of Wildlife Resources for their support of this research, Drs. Yasir Kaheil and Enrique Rosero for their assistance and insight, and Dr. Anders Wörman for his thoughtful comments regarding the manuscript.

References

Battin, T. J., L. A. Kaplan, S. Findlay, C. S. Hopkinson, E. Marti, A. I. Packman, D. J. Newbold, and F. Sabater (2008), Biophysical controls on organic carbon fluxes in fluvial networks, *Nature Geoscience*, *1*, 95-100.

Bencala, K. E., and R. A. Walters (1983), Simulation of solute transport in a mountain pool-and-riffle stream: a transient storage model, *Water Resources Research*, *19*(3), 718-724.

Bencala, K. E., R. E. Rathbun, A. P. Jackman, V. C. Kennedy, G. W. Zellweger, and R. J. Avanzino (1983), Rhodamine WT dye losses in a mountain stream environment, *Water Resources Bulletin American Water Resources Association*, *19*(6), 943-950.

Bingham, Q. G. (2009), Data Collection and Analysis Methods for Two-Zone Temperature and Solute Model Parameter Estimation and Corroboration, 102 pp, Utah State University, Logan, UT.

Briggs, M. A., M. N. Gooseff, C. D. Arp, and M. A. Baker (2009), A Method for Estimating Surface Transient Storage Parameters for Streams with Concurrent Hyporheic Exchange, *Water Resources Research*, *45*, W00D27.

Cardenas, M. B., J. L. Wilson, and R. Haggerty (2008), Residence time of bedform-driven hyporheic exchange, *Advances in Water Resources*, *31*, 1382-1386.

Chapra, S. C., and R. L. Runkel (1999), Modeling Impact of Storage Zones on Stream Dissolved Oxygen, *Journal of Environmental Engineering*, *125*(5), 415-419.

Choi, J., J. W. Harvey, and M. H. Conklin (2000), Characterizing multiple timescales of stream and storage zone interaction that affect solute fate and transport in streams, *Water Resources Research*, *36*(6), 1511-1518.

D'Angelo, D. J., J. R. Webster, S. V. Gregory, and J. L. Meyer (1993), Transient storage in Appalachian and Cascade mountain streams as related to hydraulic characteristics, *Journal of North American Benthological Society*, *12*(3), 223-235.

Duan, Q., S. Sorooshian, and V. Gupta (1992), Effective and efficient global optimization for conceptual rainfall-runoff models, *Water Resources Research*, *28*(4), 1015-1031.

Dunckel, A. E., M. B. Cardenas, A. H. Sawyer, and P. C. Bennett (2009), High-resolution in-situ thermal imaging of microbial mats at El Tatio Geyser, Chile shows coupling between community color and temperature, *Geophysical Research Letters*, *36*(L23403), 5.

Everts, C. J., and R. S. Kanwar (1994), Evaluation of Rhodamine WT as an absorbed tracer in an agricultural soil, *Journal of Hydrology*, *153*, 53-70.

Gooseff, M. N., S. M. Wondzell, R. Haggerty, and J. Anderson (2003), Comparing transient storage modeling and residence time distribution (RTD) analysis in geomorphically varied reaches in the Lookout Creek basin, Oregon, USA, *Advances in Water Resources*, *26*, 925 - 937.

Gupta, H. V., S. Sorooshian, and P. O. Yapo (1998), Toward Improved Calibration of Hydrologic Models: Multiple and Noncommensurable Measures of Information, *Water Resources Research*, *34*(4), 751-763.

Haggerty, R., S. M. Wondzell, and M. A. Johnson (2002), Power-law residence time distribution in the hyporheic zone of a 2nd-order stream, *Geophysical Research Letters*, *29*(13), 4.

Harvey, J. W., and B. J. Wagner (2000), Streams and Ground Waters, in *Aquatic Ecology Series*, edited by J. B. Jones and P. J. Mulholland, p. 425, Academic Press, San Diego.

Harvey, J. W., B. J. Wagner, and K. E. Bencala (1996), Evaluating the reliability of the stream tracer approach to characterize stream-subsurface water exchange, *Water Resources Research*, *32*(8), 2441-2451.

Harvey, J. W., J. E. Saiers, and J. T. Newlin (2005), Solute transport and storage mechanisms in wetlands of the Everglades, south Florida, *Water Resources Research*, *41*(W05009), 1-14.

Jones, J. B., and P. J. Mulholland (2000), *Streams and Ground Waters*, 425 pp., Academic Press, San Diego.

Laenen, A., and K. E. Bencala (2001), Transient storage assessments of dye-tracer injections in rivers of the Willamette Basin, Oregon, *Journal of the Amercian Water Resources Association*, *37*(2), 367-377.

Legates, D. R., and G. J. McCabe, Jr. (1999), Evaluating the use of goodness-of-fit measures in hydrologic and hydroclimatic model validation, *Water Resources Research*, *35*(1), 233-241.

Lin, A. Y.-C., J.-F. Debroux, J. A. Cunningham, and M. Reinhard (2003), Comparison of rhodamine WT and bromide in the determination of hydraulic characteristics of constructed wetlands, *Ecological Engineering*, *20*, 75-88.

Loheide, S. P., and S. M. Gorelick (2006), Quantifying stream-aquifer interactions through the analysis of remotely sensed thermographic profiles in in situ temperature histories, *Environmental Science and Technology*, *40*(10), 3336-3341.

Neilson, B. T., D. K. Stevens, S. C. Chapra, and C. Bandaragoda (2009), Data Collection Methodology for Dynamic Temperature Model Testing and Corroboration, *Hydrological Processes*, *23*, 2902-2914.

Neilson, B. T., D. K. Stevens, S. C. Chapra, and C. Bandaragoda (2010), Two zone transient storage modeling using temperature and solute data with multiobjective calibration: Part 1 Temperature, *Water Resources Research*, *329*, 26-38.

Runkel, R. L. (1998), One dimensional transport with inflow and storage (OTIS): A solute transport model for streams and rivers*Rep. 98-4018*, 73 pp, U.S. Geological Survey.

Runkel, R. L., and D. M. McKnight (2003), Preface: Modeling hyporheic zone processes, *Advances in Water Resources*, *26*, 901-905.

Selker, J. S., N. Van de Giesen, M. Westhoff, W. Luxemburg, and M. B. Parlange (2006a), Fiber optics opens window on stream dynamics, *Geophysical Research Letters*, *33*(L24401).

Selker, J. S., L. Thevenaz, H. Huwald, M. Alfred, W. Luxemburg, N. van de Giesen, M. Stejskal, J. Zeman, M. Westhoff, and M. B. Parlange (2006b), Distributed fiber-optic temperature sensing for hydrologic systems, *Water Resources Research*, *42*(W12202), 8.

Shiau, B.-J., D. A. Sabatini, and J. H. Harwell (1993), Influence of rhodamine WT properties on sorption and transport in subsurface media, *Ground Water*, *31*(6), 913-920.

Torgersen, C. E., R. N. Faux, B. A. McIntosh, N. J. Poage, and D. J. Norton (2001), Airborne thermal remote sensing for water temperatures assessment in rivers and streams, *Remote Sensing of the Environment*, *76*, 386-398.

Vrugt, J. A., H. V. Gupta, W. Bouten, and S. Sorooshian (2003a), A shuffled complex evolution metropolis algorithm for optimization and uncertainty assessment of hydrologic model parameters., *Water Resources Research*, *39*(8), 1201.

Vrugt, J. A., H. V. Gupta, L. A. Bastidas, W. Bouten, and S. Sorooshian (2003b), Effective and efficient algorithm for multiobjective optimization of hydrologic models, *Water Resources Research*, *39*(8), 1214.

Wagner, B. J., and J. W. Harvey (1997), Experimental design for estimating parameters of rate-limited mass transfer: Analysis of stream tracer studies., *Water Resources Research*, *33*(7), 1731-1741.

Westhoff, M. C., H. H. G. Savenije, W. M. J. Luxemburg, G. S. Stelling, N. C. Van de Giesen, J. S. Selker, L. Pfister, and S. Uhlenbrook (2007), A distributed stream temperature model using high resolution temperature observations., *Hydrology and Earth Systems Sciences*, *11*, 1469-1480.

Worman, A., J. Forsman, and H. Johansson (1998), Modeling retention of sorbing solutes in streams based on tracer experiment using 51Cr, *Journal of Environmental Engineering*, *124*(2), 122-130.

Worman, A., A. I. Packman, H. Johansson, and K. Jonsson (2002), Effect of flow-induced exchange in hyporheic zone on longitudinal transport of solutes in stream and rivers, *Water Resources Research*, *38*(1), 15.

Zaramella, M., and A. I. Packman (2003), Application of the transient storage model to analyze advective hyporheic exchange with deep and shallow sediment beds, *Water Resources Research*, *39*(7), 1198.

Zaramella, M., A. Marion, and A. I. Packman (2006), Applicability of the Transient Storage Model to the hyporheic exchange of metals., *Journal of Contaminant Hydrology*, *84*, 21-35.

Table and Figure Captions

Table 1. Virgin River one-zone modeling information and parameters.

Table 2. Resulting best parameter sets for all three two-objective optimizations.

Figure 1. Solute tracer data collected as CS 3 in the MC and STS in July 2005.

Figure 2. Simulation results for: (a) MC temperatures at CS 2, (b) MC temperatures at CS 3, (c) MC tracer concentrations at CS 3, and (d) STS tracer concentrations at CS 3 from parameter sets corresponding to $NSE > 0.9$ for the MC temperatures at CS 2. The shaded areas contain model bounds for $NSE > 0.9$ for the MC temperatures at CS 2. The symbols represent observations.

Figure 3. Simulation results for (a) MC temperatures at CS 2, (b) MC temperatures at CS 3, (c) MC tracer concentrations at CS 3, and (d) STS tracer concentrations at CS 3 from parameter sets corresponding to $NSE > 0.9$ for the MC temperatures at CS 3. The shaded areas contain model bounds for $NSE > 0.9$ for the MC temperatures at CS 3. The symbols represent observations.

Figure 4. Simulation results for (a) MC temperatures at CS 2, (b) MC temperatures at CS 3, (c) MC tracer concentrations at CS 3, and (d) STS tracer concentrations at CS 3 from parameter sets corresponding to $NSE > 0.9$ for the MC tracer concentrations at CS 3. The shaded areas contain model bounds for $NSE > 0.9$ for the MC tracer concentrations at CS 3. The symbols represent observations.

Figure 5. Model results from the "best" parameter set and observations for all zones given a two-objective optimization using MC temperatures at CS 2 and MC temperatures at CS 3. Model results are shown as solid gray lines. Observed temperature time series are shown as solid black lines in (a) and (b). Observed STS time series are plotted as solid (temperature probe 1, river left) and dashed (temperature probe 1, river right) black lines in (d) and (e). Three observed time series are plotted in (g) and (h) as three different black line types corresponding to 3cm (temperature probe 5, solid line), 9 cm (temperature probe 6, dashed line), and 20 cm (temperature probe 7, dotted line). Tracer observations are plotted as symbols (circles for MC, squares for STS 1, and triangles for STS 2) in (c) and (f).

Figure 6. Model result bounds for all Pareto solutions plotted with observations for all zones and locations given a two-objective optimization using MC temperatures at CS 2 and MC temperatures at CS 3. Model results are shown as solid gray bounds. Observed temperature time series are shown as solid black lines in (a) and (b). Observed STS time series are plotted as solid (temperature probe 1, river left) and dashed (temperature probe 1, river right) black lines in (d) and (e). Three observed time series are plotted in (g) and (h) as three different black line types corresponding to 3 cm (temperature probe 5, solid line), 9 cm (temperature probe 6, dashed line), and 20 cm (temperature probe 7, dotted line). Tracer

observations are plotted as symbols (circles for MC, squares for STS 1, and triangles for STS 2) in (c) and (f).

Figure 7. Model results and observations for all zones given a two-objective optimization using MC tracer concentrations at CS 3 and STS2 tracer concentrations at CS 3. Model results are shown as solid gray lines. Observed temperature time series are shown as solid black lines in (a) and (b). Observed STS time series are plotted as solid (temperature probe 1, river left) and dashed (temperature probe 1, river right) black lines in (d) and (e). Three observed time series are plotted in (g) and (h) as three different black line types corresponding to 3cm (temperature probe 5, solid line), 9 cm (temperature probe 6, dashed line), and 20 cm (temperature probe 7, dotted line). Tracer observations are plotted as symbols (circles for MC, squares for STS 1, and triangles for STS 2) in (c) and (f).

Figure 8. Model results and observations for all zones given a two-objective optimization using MC tracer concentrations at CS 3 and MC temperatures at CS 3. Model results are shown as solid gray lines. Observed temperature time series are shown as solid black lines in (a) and (b). Observed STS time series are plotted as solid (temperature probe 1, river left) and dashed (temperature probe 1, river right) black lines in (d) and (e). Three observed time series are plotted in (g) and (h) as three different black line types corresponding to 3cm (temperature probe 5, solid line), 9 cm (temperature probe 6, dashed line), and 20 cm (temperature probe 7, dotted line). Tracer observations are plotted as symbols (circles for MC, squares for STS 1, and triangles for STS 2) in (c) and (f).

Figure 9. Model result bounds for all Pareto solutions plotted with observations for all zones and locations given a two-objective optimization using MC tracer concentrations at CS 3 and MC temperatures at CS 3. Model results are shown as solid gray bounds. Observed temperature time series are shown as solid black lines in (a) and (b). Observed STS time series are plotted as solid (temperature probe 1, river left) and dashed (temperature probe 1, river right) black lines in (d) and (e). Three observed time series are plotted in (g) and (h) as three different black line types corresponding to 3cm (temperature probe 5, solid line), 9 cm (temperature probe 6, dashed line), and 20 cm (temperature probe 7, dotted line). Tracer observations are plotted as symbols (circles for MC, squares for STS 1, and triangles for STS 2) in (c) and (f).

Table 1. Virgin River one-zone modeling information and parameters.

		Upper Section	**Lower Section**
Flow MC	Q_{MC}	2.861	3.143
Total Channel Width (m)	B_{tot}	29.9	23.5
Manning Roughness	n	0.06	0.05
Depth MC (m)	Y_{MC}	0.24	0.38
% Total Channel Width TS	β	18.8	25.0
Cross Sectional Area (m^2) TS	$A_{c,TS}$	1.33	7.90
TS Exchange Coefficient ($m^2\ s^{-1}$)	α_{TS}	1.19E-03	4.19E-04
Depth TS (m)	Y_{TS}	0.236	1.349
DaI (One Zone Model)	DaI	1.8	1.1

Table 2. Resulting best parameter sets for all three two-objective optimizations.

		Temperature MC CS 2 and MC CS 3		**Tracer MC and STS CS 3**		**Temperature MC and Tracer MC CS 3**	
Parameter Description	**Parameter Name**	**Upper Section**	**Lower Section**	**Upper Section**	**Lower Section**	**Upper Section**	**Lower Section**
Total Channel Width (m)	B_{tot}	22	16	21	20	15	22
Manning Roughness	n	0.060	0.026	0.050	0.059	0.060	0.027
STS Width (% Total Channel Width)	β	30	30	6	30	30	8
STS CS Area (m^2)	$A_{c,STS}$	2.00	0.51	0.95	0.55	1.95	1.93
STS Diffusivity (m^2 d^{-1})	α_{STS}	$6.30x10^4$	$1.96x10^4$	$4.40x10^4$	$2.35x10^4$	$7.03x10^4$	$8.46x10^4$
HTS Advective Transport Coefficient (m^3 d^{-1})	Q_{HTS}	864	863	226	174	179	861
Depth of HTS (m)	Y_{HTS}	0.45	0.99	0.05	0.99	0.29	0.88
Depth of Ground Conduction (m)	Y_{gr}	1.00	1.00	0.89	0.89	0.84	0.84

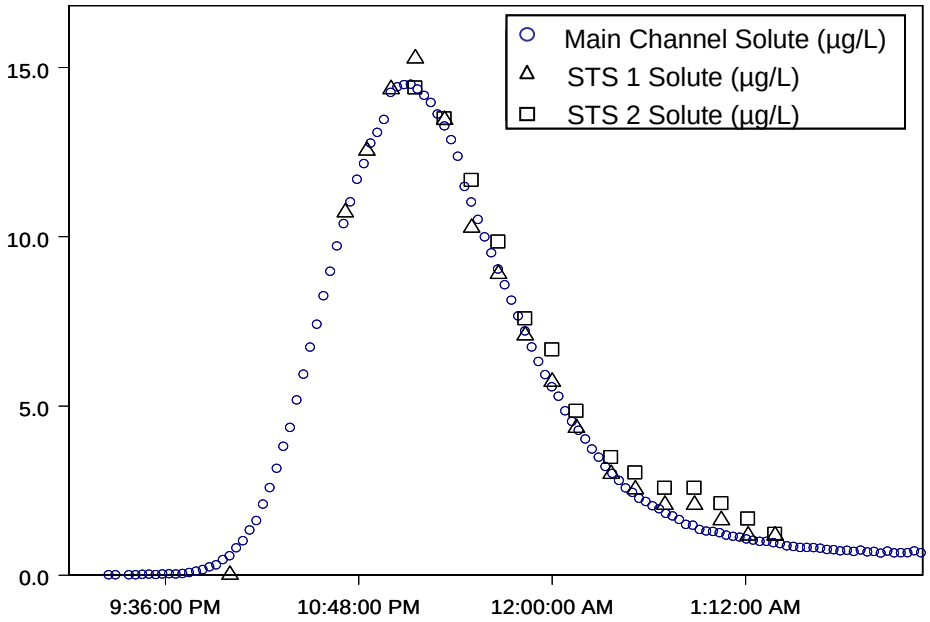

Figure 1. Solute tracer data collected as CS 3 in the MC and STS in July 2005.

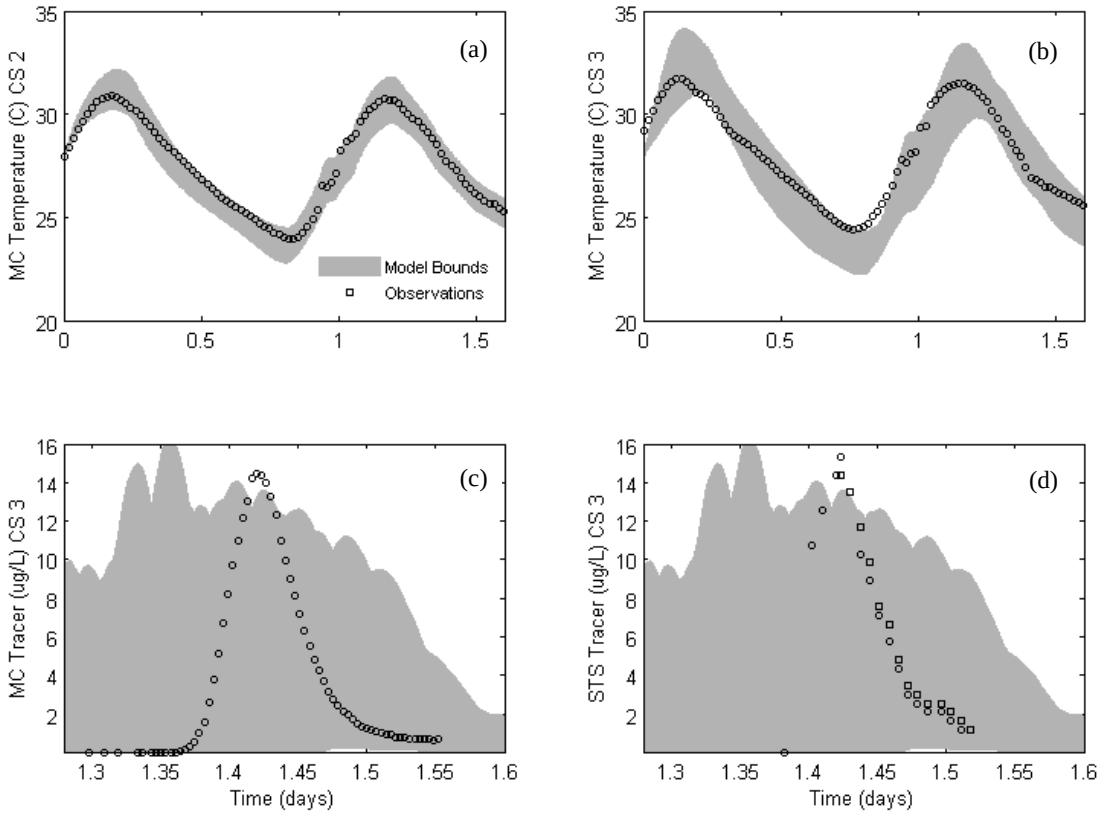

Figure 2. Simulation results for: (a) MC temperatures at CS 2, (b) MC temperatures at CS 3, (c) MC tracer concentrations at CS 3, and (d) STS tracer concentrations at CS 3 from parameter sets corresponding to *NSE* > 0.9 for the MC temperatures at CS 2. The shaded areas contain model bounds for *NSE* > 0.9 for the MC temperatures at CS 2. The symbols represent observations.

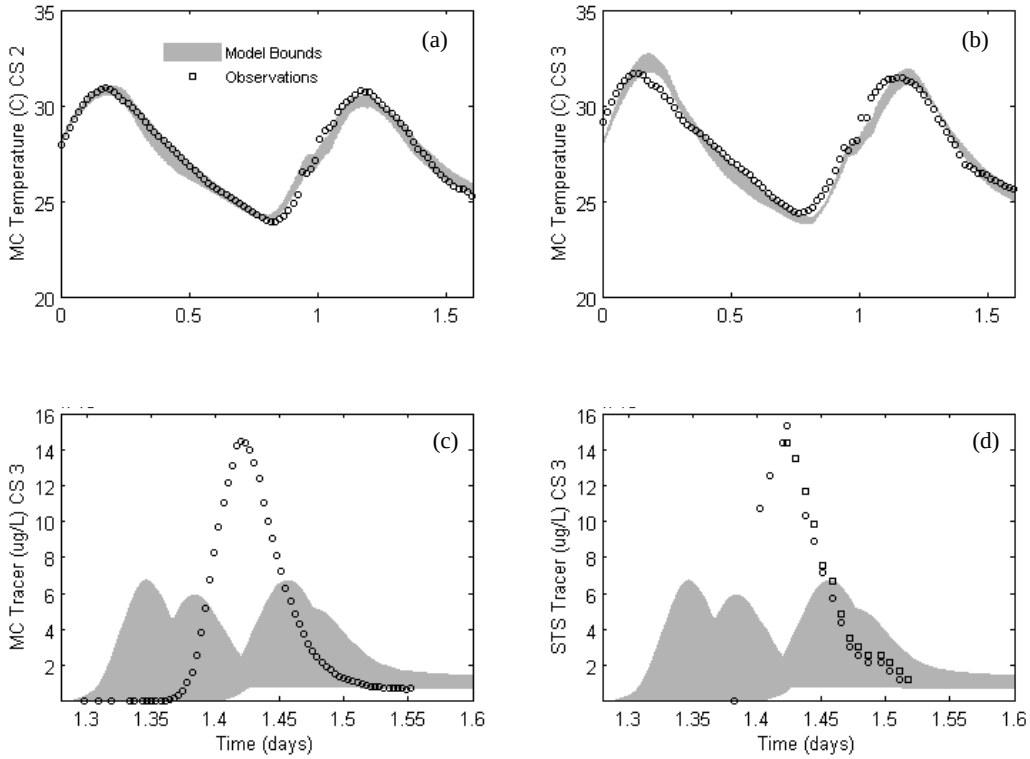

Figure 3. Simulation results for (a) MC temperatures at CS 2, (b) MC temperatures at CS 3, (c) MC tracer concentrations at CS 3, and (d) STS tracer concentrations at CS 3 from parameter sets corresponding to *NSE* > 0.9 for the MC temperatures at CS 3. The shaded areas contain model bounds for *NSE* > 0.9 for the MC temperatures at CS 3. The symbols represent observations.

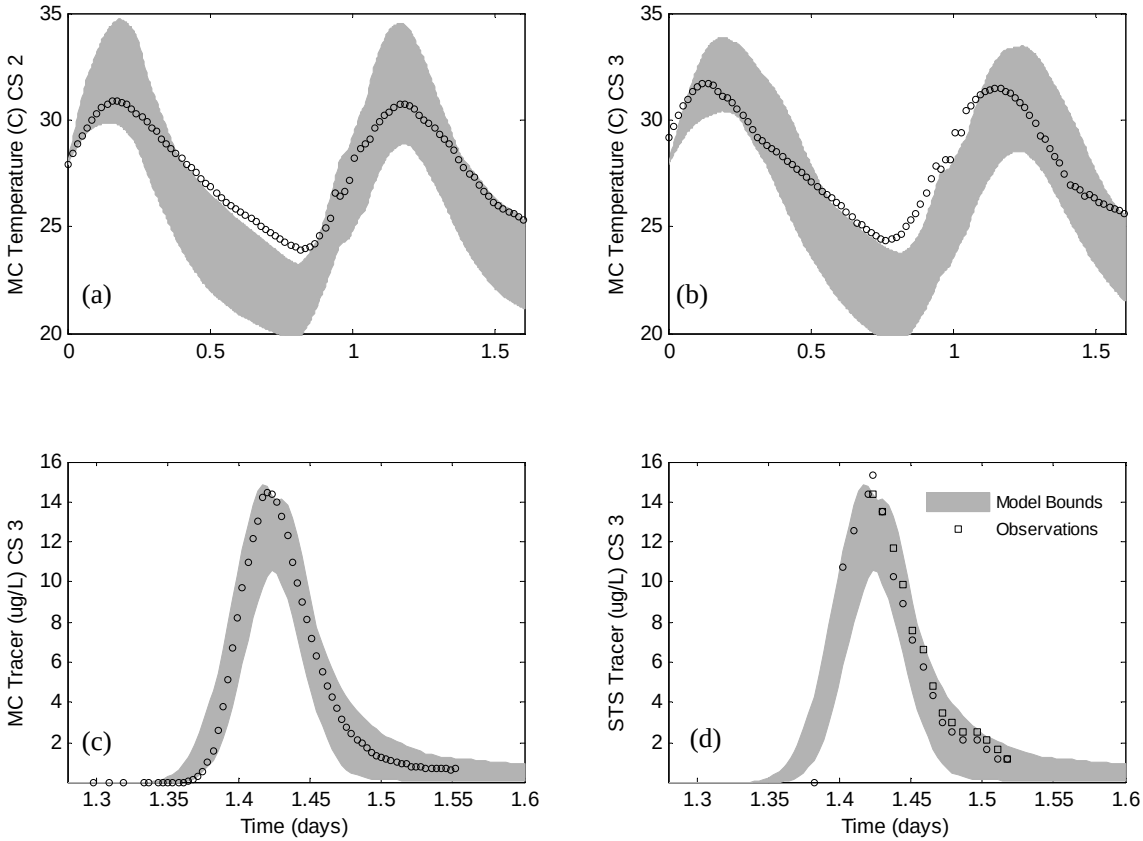

Figure 4. Simulation results for (a) MC temperatures at CS 2, (b) MC temperatures at CS 3, (c) MC tracer concentrations at CS 3, and (d) STS tracer concentrations at CS 3 from parameter sets corresponding to *NSE* > 0.9 for the MC tracer concentrations at CS 3. The shaded areas contain model bounds for *NSE* > 0.9 for the MC tracer concentrations at CS 3. The symbols represent observations

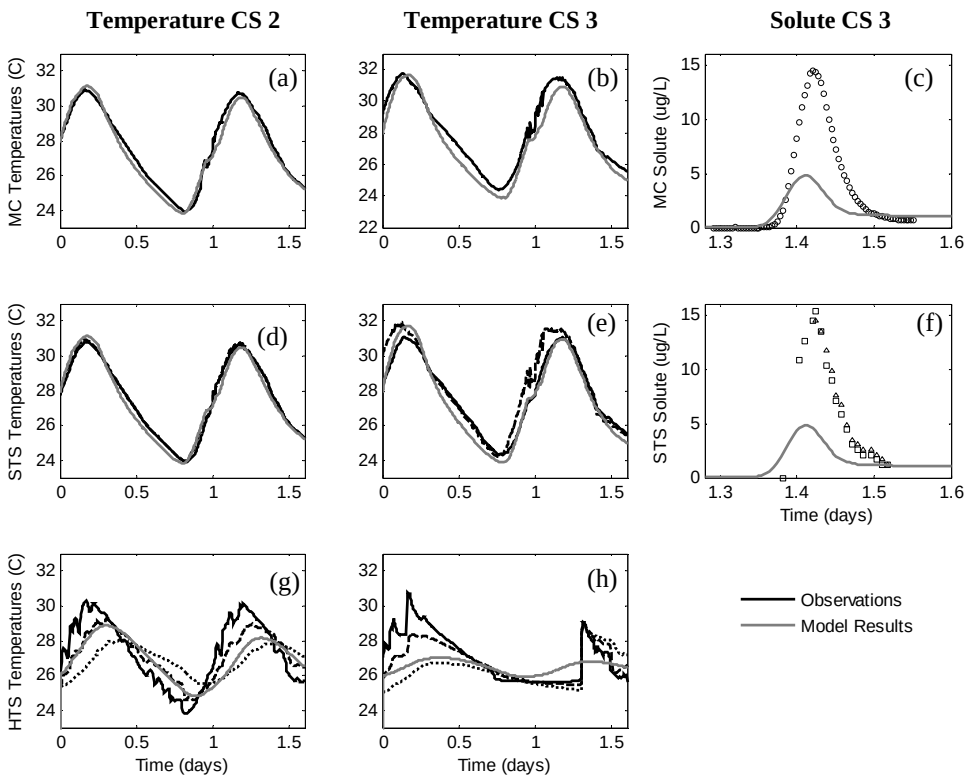

Figure 5. Model results from the "best" parameter set and observations for all zones given a two-objective optimization using MC temperatures at CS 2 and MC temperatures at CS 3. Model results are shown as solid gray lines. Observed temperature time series are shown as solid black lines in (a) and (b). Observed STS time series are plotted as solid (temperature probe 1, river left) and dashed (temperature probe 1, river right) black lines in (d) and (e). Three observed time series are plotted in (g) and (h) as three different black line types corresponding to 3cm (temperature probe 5, solid line), 9 cm (temperature probe 6, dashed line), and 20 cm (temperature probe 7, dotted line). Tracer observations are plotted as symbols (circles for MC, squares for STS 1, and triangles for STS 2) in (c) and (f).

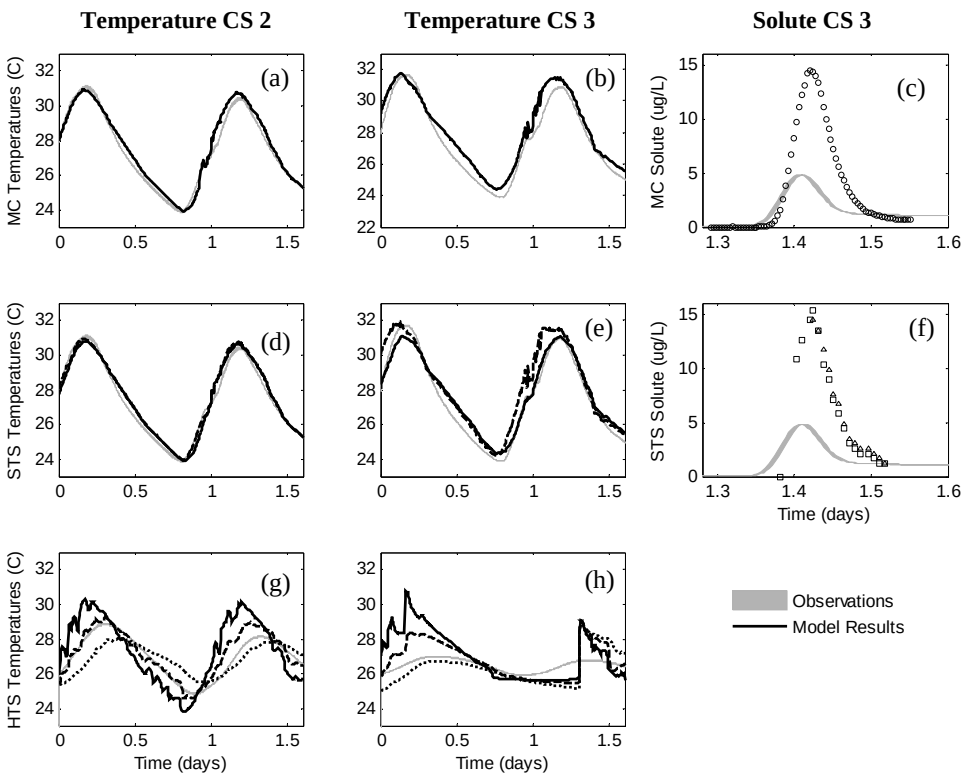

Figure 6. Model result bounds for all Pareto solutions plotted with observations for all zones and locations given a two-objective optimization using MC temperatures at CS 2 and MC temperatures at CS 3. Model results are shown as solid gray bounds. Observed temperature time series are shown as solid black lines in (a) and (b). Observed STS time series are plotted as solid (temperature probe 1, river left) and dashed (temperature probe 1, river right) black lines in (d) and (e). Three observed time series are plotted in (g) and (h) as three different black line types corresponding to 3 cm (temperature probe 5, solid line), 9 cm (temperature probe 6, dashed line), and 20 cm (temperature probe 7, dotted line). Tracer observations are plotted as symbols (circles for MC, squares for STS 1, and triangles for STS 2) in (c) and (f).

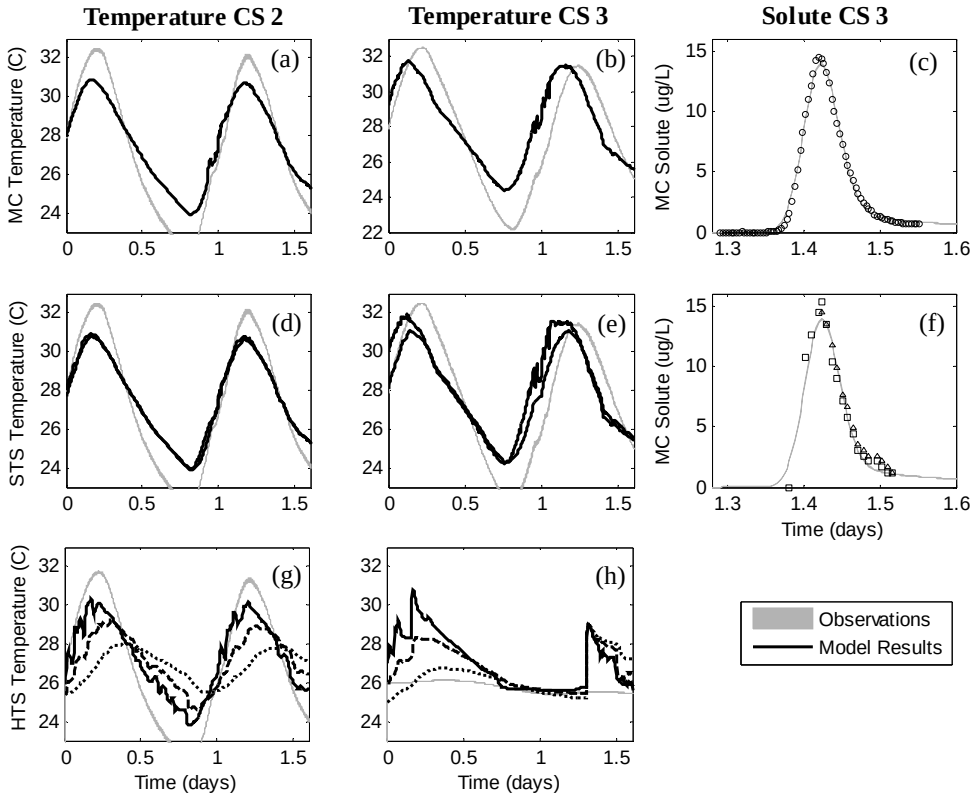

Figure 7. Model results and observations for all zones given a two-objective optimization using MC tracer concentrations at CS 3 and STS2 tracer concentrations at CS 3. Model results are shown as solid gray lines. Observed temperature time series are shown as solid black lines in (a) and (b). Observed STS time series are plotted as solid (temperature probe 1, river left) and dashed (temperature probe 1, river right) black lines in (d) and (e). Three observed time series are plotted in (g) and (h) as three different black line types corresponding to 3cm (temperature probe 5, solid line), 9 cm (temperature probe 6, dashed line), and 20 cm (temperature probe 7, dotted line). Tracer observations are plotted as symbols (circles for MC, squares for STS 1, and triangles for STS 2) in (c) and (f).

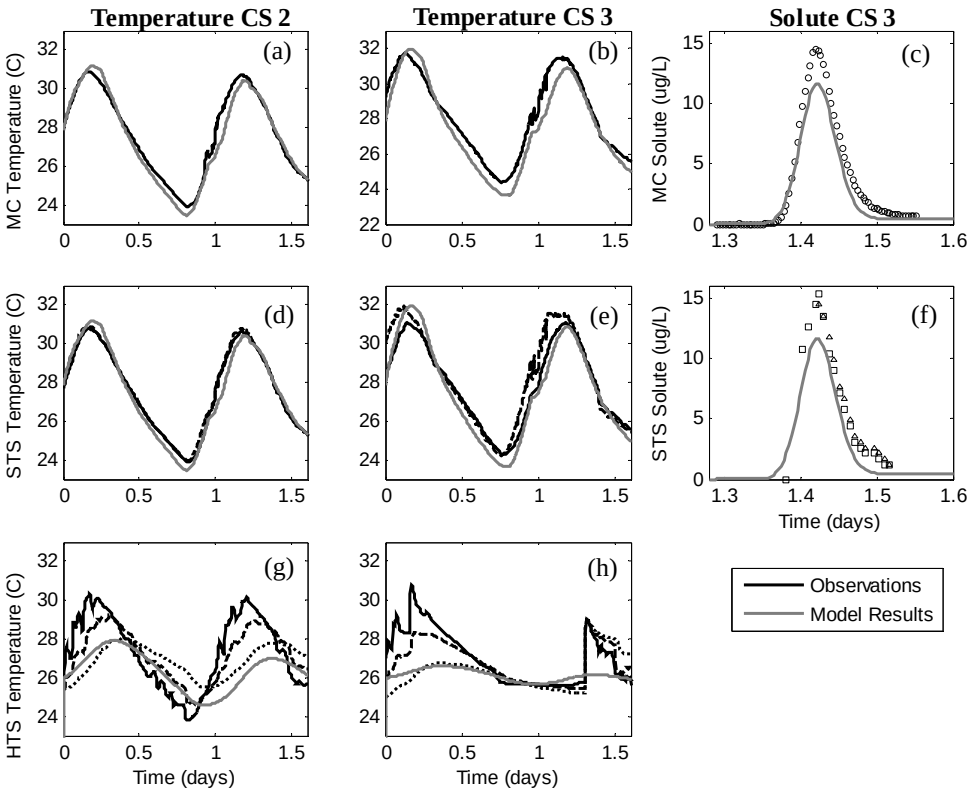

Figure 8. Model results and observations for all zones given a two-objective optimization using MC tracer concentrations at CS 3 and MC temperatures at CS 3. Model results are shown as solid gray lines. Observed temperature time series are shown as solid black lines in (a) and (b). Observed STS time series are plotted as solid (temperature probe 1, river left) and dashed (temperature probe 1, river right) black lines in (d) and (e). Three observed time series are plotted in (g) and (h) as three different black line types corresponding to 3cm (temperature probe 5, solid line), 9 cm (temperature probe 6, dashed line), and 20 cm (temperature probe 7, dotted line). Tracer observations are plotted as symbols (circles for MC, squares for STS 1, and triangles for STS 2) in (c) and (f).

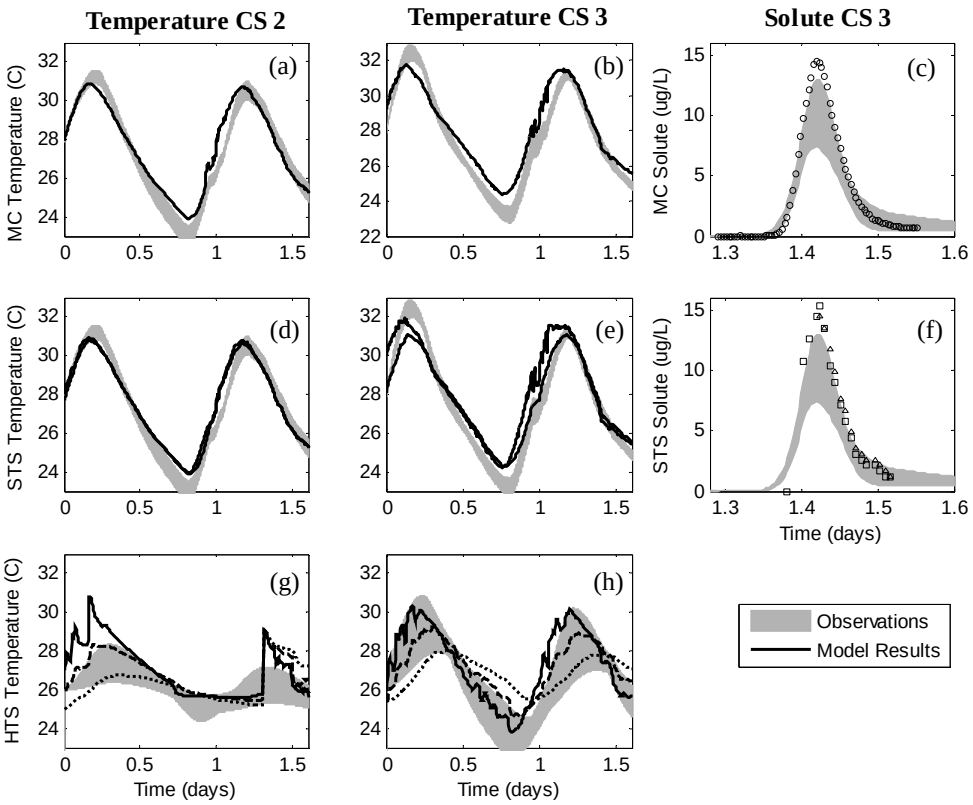

Figure 9. Model result bounds for all Pareto solutions plotted with observations for all zones and locations given a two-objective optimization using MC tracer concentrations at CS 3 and MC temperatures at CS 3. Model results are shown as solid gray bounds. Observed temperature time series are shown as solid black lines in (a) and (b). Observed STS time series are plotted as solid (temperature probe 1, river left) and dashed (temperature probe 1, river right) black lines in (d) and (e). Three observed time series are plotted in (g) and (h) as three different black line types corresponding to 3cm (temperature probe 5, solid line), 9 cm (temperature probe 6, dashed line), and 20 cm (temperature probe 7, dotted line). Tracer observations are plotted as symbols (circles for MC, squares for STS 1, and triangles for STS 2) in (c) and (f).